Cystic fibrosis patient-derived bronchial organoids unveil druggable pathways against *Mycobacterium abscessus* infection

Stephen Adonai Leon-Icaza[1], Salimata Bagayoko[1], Nino Iakobachvili[2], Chloé Ferrand[1], Talip Aydogan[3], Celia Bernard[1], Angelique Sanchez Dafun[1], Marlène Murris-Espin[4], Julien Mazières[4], Pierre Jean Bordignon[1], Serge Mazères[1], Pascale Bernes-Lasserre[5], Victoria Ramé[5], Jean-Michel Lagarde[5], Julien Marcoux[1], Marie Pierre Bousquet[1], Christian Chalut[1], Christophe Guilhot[1], Hans Clevers[6], Peter J. Peters[2], Virginie Molle[3], Geanncarlo Lugo-Villarino[1], Kaymeuang Cam[1], Laurence Berry[3], Etienne Meunier[1], Céline Cougoule[1*]

[1]Institut de Pharmacologie et de Biologie Structurale (IPBS), Université de Toulouse, CNRS, UPS, Toulouse, France

[2]M4i Nanoscopy Division, Maastricht University, Maastricht, Netherlands

[3]Laboratory of Pathogen Host Interactions (LPHI), Université Montpellier, CNRS, Montpellier, France

[4]Service de Pneumologie, Hôpital Larrey, CHU de Toulouse, Toulouse, France

[5] Imactiv-3D SAS, 1 Place Pierre POTIER, 31100 Toulouse, France

[6]Oncode Institute, Hubrecht Institute, Royal Netherlands Academy of Arts and Sciences and University Medical Center, Utrecht, Netherlands

Correspondance

Céline Cougoule, Institut de Pharmacologie et Biologie Structurale (IPBS), Université de Toulouse, CNRS, UPS, Toulouse, France. Email: Celine.Cougoule@ipbs.fr

Author contributions

Conceptualization and methodology: SALI, SB, NI, CF, TA, M. M-E, JM, P-J.B, CB, ASD, PBL, VR, JML, JM, MPB, CCh, CG, HC, P-J P, G.L-V, VM, KC, LB, EM and CCo; Investigation: SALI, SB, NI, CF, TA, P-J.B, CB, CCh, KC, LB, and CCo. Resources: CG, HC, M. M-E, JM, J-M L., HC, P-J P, VM, LB, EM and CCo; Funding acquisition: P-J P., G L-V, , LB, EM and CCo;

Grant support

This project has been funded by grants from “Vaincre La Mucoviscidose” and “Grégory Lemarchal” foundations (N°RF20210502852/1/1/48) to CC, from the “Fondation pour la Recherche Médicale” (FRM) and ERC StG (INFLAME) to EM. SALI was funded by “Vaincre La Mucoviscidose” PhD fellowship (N°RF20210502852/1/1/48). This work was also supported by grants from CNRS (IEA 300134) to CC, Campus France PHC Van Gogh (40577ZE) to GL-V, ZonMW 3R’s (114021005) to PJP, the Nuffic Van Gogh Programme (VGP.17/10 to NI), and by the LINK program from the Province of Limburg, the Netherlands. TA, VM and LB were funded by "La Région Languedoc-Roussillon" (N° DRTE/RSS - ESR_R&S_DF-000061-2018-003268).

Funders had no interference in the conduct of the project.

Competing Interest Statement: H.C is inventor on patents related to organoid technology. Other authors declare no conflict of interest, his full disclosure is given at https://www.uu.nl/staff/JCClevers/.

Abstract

Mycobacterium abscessus (Mabs) drives life-shortening mortality in cystic fibrosis (CF) patients, primarily because of its resistance to chemotherapeutic agents. Both our knowledge on and models to investigate the host and bacterial determinants that drive Mabs pathology in CF patients remain rudimentary. Here, we evaluated whether the lung organoid technology from CF patients is appropriate for modelling Mabs infection and whether antioxidant treatment is a candidate therapeutic approach in the context of CF disease. We derived airway organoids (AOs) from lung biopsy of a CF patient and characterized these AO by assessing CF transmembrane conductance regulator (CFTR) function, mucus and reactive oxygen species (ROS) production, lipid peroxidation, and cell death. We microinjected smooth (S-) or rough (R-)Mabs in the lumen of AOs to evaluate its fitness, responses of AOs to infection, and treatment efficacy by colony forming unit assay, qPCR and microscopy. We show that CF patient-derived AOs exhibited low residual CFTR function, enhanced mucus accumulation, and increased oxidative stress, lipid peroxidation, and cell death at basal state. While in AOs, S Mabs formed biofilm, R Mabs formed cord serpentines and displayed a higher virulence. S and R Mabs replicated more efficiently in CF AOs than in AOs derived from healthy lung. Pharmacological activation of antioxidant pathways resulted in better control of Mabs growth. In conclusion, we have established CF patient-derived AOs as a suitable human system to decipher mechanisms of CF-enhanced respiratory infection by Mabs and confirmed antioxidant approaches as a potential host-directed strategy to improve Mabs infection control.

Introduction

Cystic Fibrosis (CF) is due to mutations in the CF transmembrane conductance regulator (CFTR) gene (1), which regulates ion transport, that impair lung mucociliary clearance and result in pathological triad hallmarks of CF, i.e., chronic airway mucus build-up, sustained inflammation, and microbe trapping leading to parenchyma epithelial cell destruction. The major reason CF patients succumbing to this disease is respiratory failure resulting from chronic lung infection (2).

CF Patients have a greater risk of infection by Non-Tuberculous Mycobacteria (NTM), mainly by the most virulent and drug-resistant NTM *Mycobacterium abscessus* (Mabs) (3) (4). Mabs display two distinct morphotypes based on the presence or absence of glycopeptidolipids (GPL) in their cell wall (5). The smooth (S) GPL-expressing variant forms biofilm and is associated with environmental isolates. The Rough (R) variant does not express GPL, forms cording and induces more aggressive and invasive pulmonary disease, particularly in CF patients (5–7). In CF patients, Mabs colonization is initiated by the infection with the S variant that, over time, switches to the R morphotype by losing or down-regulating surface GPL (8, 9). Although animal models like immunocompromised mice (10), zebrafish (11–13) and *Xenopus laevis* (14) contributed to a significant advance in the understanding of Mabs infection (15), their tissue architecture and cell composition are different from that of humans and do not recapitulate the hallmarks of CF (16–18). Models with anatomical and functional relevance to the human airway and displaying the diversity of natural CFTR gene mutations would complement other in vivo models.

Recent advances in stem cell biology have allowed the growth of human tissues *in vitro* that resemble organs *in vivo* (19–21). Human airway organoids (AOs) are derived from adult stem cells present in lung tissues (22), are self-organized 3D structures and share important characteristics with adult bronchiolar part of the human lung (22, 23). We and others have adapted AOs for modelling infectious diseases with bacteria, such as mycobacteria (24) and *Pseudomonas aeruginosa* (25), with viruses, such as RSV (22) and SARS-CoV-2 (26–28), and with parasites (29). Of

particular interest, organoids derived from CF patients constitute a unique system to model natural mutations of CFTR and its dysfunctions, thus recapitulating critical aspects of CF in human (22, 30, 31) that are not achievable with other cellular or animal models.

Here, we report the generation and characterization of an AO line derived from a CF patient that recapitulates hallmarks of human CF disease, including exacerbated oxidative stress. Both Mabs S and R infect and replicate within these AOs and display their specific features, such as forming biofilm and cording, respectively. Moreover, enhanced reactive oxygen species (ROS) production by Mabs infection or the CF context favours Mabs growth, which is reversed by antioxidant treatments.

Materials and Methods

Detailed protocols are provided in the supplement.

Ethic statements: The collection of patient data and tissue for AO generation was performed according to the guidelines of the European Network of Research Ethics Committees following European and national law. The accredited ethical committee reviewed and approved the study in accordance with the Medical Research Involving Human Subjects Act. Human lung tissue was provided by the CHU of Toulouse under protocol agreement (CHU 19 244 C and Ref CNRS 205782). All patients participating in this study consented to scientific use of their material; patients can withdraw their consent at any time, leading to the prompt disposal of their tissue and any derived material.

Airway organoid culture and maintenance

Healthy adjacent tissue from two independent donors with lung cancer, and one lung biopsy of cystic fibrosis heterozygous patient (G542X/1811+1.6kbA-->G) were used to derive organoids as previously described with minor changes (22, 24).

Microscopy

For the epithelium thickness measurement, organoids were cultured for five weeks before acquired bright field images. Assessing CFTR function was performed by forskolin-induced organoid swelling assay (5 µM, 2 hr at 37 °C) (Sigma-Aldrich, Burlington, MA, USA) as described (33). Live imaging was performed to quantify mucus accumulation with Zinpyr-1 (10 µM, overnight at 37 °C) (Santa Cruz Biotechnology, Dallas, TX, USA), ROS levels by H2DCFDA (10 µM, 30 min at 37 °C) (Invitrogen, Waltham, MA, USA) or MitoSOX (5 µM, 30 min at 37 °C) (Thermo Scientific, Waltham, MA, USA), lipid peroxidation by BODIPY (2 µM, 30 min at 37 °C; Thermo Scientific) and cell death with Propidium Iodide (50 µg ml^{-1}; Thermo Scientific) in noninfected and Mabs-infected organoids. Images were acquired under an EVOS M7000 Imaging System (10x, at 37°C with 5% CO_2) and analyzed post-acquisition with Fiji/ImageJ.

For scanning electron microscopy (SEM) and transmission electron microscopy (TEM), organoids were fixed in 2% paraformaldehyde (EMS, Hatfield, PA, USA), 2.5% glutaraldehyde (EMS) and 0.1 M Sodium Cacodylate (EMS) over night at room temperature. After, samples were embedding in Durcupan ACM resin (Sigma-Aldrich) then, semi-thin (300nm) serial sections were made using an UC7 ultramicrotome (Leica, Wetzlar, Germany) and collected on silicon wafers (Ted Pella, Redding, CA, USA). Sections were imaged on a Quanta FEG 250 SEM microscope in BSE mode. Ultrathin sections were also collected on copper grids formvar coated for TEM analysis on a JEOL 1200 EXE II Microscope.

Bacteria culture and organoid infection

Mycobacterium abscessus sensu stricto strain CIP104536T (ATCC19977T) morphotype S and R were grown as previously described (34). Before infection, AO were seeded in Matrigel (Fisher Scientific, Hampton, NH, USA) and depending on the indicated conditions, pretreated or no with 10µM of Resveratrol (Sigma-Aldrich) or Sulforaphane (Selleck Chemicals, Houston, TX, USA) for 1hr or 6hr respectively. Both antioxidants were maintained throughout the experiment and refreshed every

two days. The infection day, the bacteria were prepared for microinjection as described (24, 35) and density was adjusted to OD_{600} = 0.1-0.4. Injected organoids were individually collected, washed in PBS 1x and embedded into fresh matrix. Injected organoids were cultured for 3-4 day if not stated otherwise.

RT-qPCR and Colony forming unit assay

Organoids were collected at day 4 post-infection or stimulation and processed as reported (24). Primer sequences are provided in supplementary Table E1.

Statistics

Statistical analyses were performed using Prism 8 and 5 (GraphPad Software). Data were compared by Mann-Whitney or unpaired T test and results reported as mean with SD. Data statistically significant was represented by *P<0.05; **P<0.01; ***P<0.001 and **** P<0.0001.

Results

AOs recapitulate hallmarks of cystic fibrosis, and display enhanced oxidative stress

We adapted the published protocol to generate AOs using lung biopsies (22, 24) obtained from a CF patient carring heterozygous G542X/1811+1.6kbA-->G mutations who underwent lung transplantation. Characterization of CF versus healthy AOs showed that CF AOs displayed a thicker epithelium (Figures 1A-B, Sup Fig. 1A), abolished swelling in the forskolin assay (Figure 1C) denoting CFTR channel malfunction, and an exacerbated accumulation of mucus in the lumen (Figures 1D-E, Sup Fig. 1A). The increased accumulation of mucus was confirmed by the increased expression of mucin genes at both the mRNA level (Supp Figure 1B) and the protein level (Figure 1F). A gene ontology enrichment study revealed the upregulation of the cellular oxidant detoxification pathway in CF AOs (fold-change 11.6; p-value 3.55e-2; Supp Figure 1C). To further evaluate the oxidative status in the CF context, healthy and CF AOs were stained with MitoSOX or H2DCFDA to detect

mitochondrial ROS and H_2O_2 production, respectively. The ROS production was enhanced in CF AOs compared to healthy ones (Figures 1G-I), which was further exacerbated after treatment with the oxidative stress inducer tert-Butyl hydroperoxide (tBHP) (41) (Sup Fig. 1B). Because high ROS levels induce lipid peroxidation leading to cell death (42–44), we examined and quantified these processes by microscopy using BODIPY (measuring lipid peroxidation) or propidium iodide (measuring cell death) and found that levels of peroxidized lipids (Figures 1J-K) and cell death (Figure 1L, Sup Fig. 1C) were higher in CF AOs than in healthy AOs.

Altogether, these results showed that organoids derived from CF lung tissue exhibited not only CFTR dysfunction and exacerbated mucus accumulation but also an increased oxidative stress, therefore representing a suitable *ex vivo* model to investigate CF-driven respiratory infections.

AOs support S- and R-Mabs replication and phenotype

To investigate whether AOs can be used for modelling Mabs infection *in vitro*, we infected healthy AOs with S- and R- Mabs variants as previously described (24). To examine whether Mabs could replicate within AOs, we quantified bacterial load in AOs overtime by colony forming unit (CFU) (Figure 2A). After a latency phase of 2 days, both Mabs S and R propagated over 12 days. Based on these data, we decided to perform experiments at 4 days post-infection, corresponding to bacteria exponential growth phase. When analysed microscopically, we observed that bacteria mainly reside in the lumen of AOs and did not detect obvious alteration of the architecture of Mabs-infected organoids compared to mock injected organoids (Figure 2B-C, supp fig 2, supp movies 1 & 2). Interestingly, we observed that S bacteria formed aggregates in the lumen of the organoids whereas R variant formed the characteristic serpentine cords (Figure 2B-C) observed *in vitro* and *in vivo* (34). To further characterize the interaction of Mabs with airway epithelial cells S- and R-Mabs-infected AOs were analysed by SEM and then TEM (Figure 2D). As previously described (22), the organoid epithelium is composed of ciliated and goblet cells (Figure 2D, 1st row). As expected, Mabs S bacilli

occupied homogeneously the organoid lumen, formed chaotically scattered aggregates (Figure 2D, 2nd row) (45). Mabs S preferentially localised in close contact with the apical side of the epithelial cells (Figure 2D, 4), particularly in the presence of cilia (Figure 2D, 3). More importantly, the same samples observed by TEM revealed that S bacteria in the lumen were surrounded by what could be an extracellular polymeric substance (46) (Figure 2D, 5), suggesting that S variant Mabs might form biofilm in the organoid lumen. We convincingly identified Mabs R forming serpentine cords, characterized by aligned bacteria, in the organoid lumen (Figure 2D, 6-8). Importantly, electron microscopy confirmed no significant internalization of Mabs by epithelial cells (24). Finally, we evaluated the virulence of S- and R-Mabs by assessing epithelial cell death. As shown in Figures 2E-F, AOs infected with the R variant exhibited enhanced cell death compared to those infected with the S variant, reflecting R bacteria hypervirulence.

Altogether, our results showed that S and R Mabs variants thrived in AOs and displayed respective features observed in *in vivo* models and in the lung of CF patients.

ROS production contributes to *Mycobacterium abscessus* growth

ROS production is an important antimicrobial process and is enhanced in the CF context, we thus evaluated whether oxidative stress played a role in Mabs fitness in AOs. We first evaluated the expression of genes related to the production and detoxification of ROS upon Mabs infection and observed increased expression of oxidases NOX1 and DUOX1, suggesting enhanced ROS production upon Mabs infection. Moreover, we observed overexpression of not only the transcription factor Nrf-2 and the Nrf-2-induced gene NQO-1, denoting Nrf-2 activation, but also detoxifying enzymes such as superoxide dismutases, PDRX1, and catalase, suggesting activation of cell protective antioxidant pathways (Figure 3A).

To confirm ROS production upon Mabs infection, Mabs-infected AOs were microscopically analysed after incubation with either MitoSOX or H2DCFDA. Both S- and R-Mabs infections enhanced the

incorporation of MitoSOX and H2DCFDA (Figures 3B-D), in agreement with the induction of ROS production. Interestingly, productions of mitochondrial ROS and H_2O_2 were higher with the R variant, further confirming R-Mabs hypervirulence compared to S-Mabs in AO.

The contribution of cell protective antioxidant pathways during mycobacterial infection remains poorly understood (49, 50). We then determined the consequence of boosting antioxidant pathways for Mabs fitness and found that treatment with either resveratrol or the Nrf-2 agonist sulforaphane reduced both S and R variant growth in AOs (Figures 3E-H).

Altogether, the results showed that, independent of the immune system, epithelial cells mounted an oxidative response upon Mabs infection, which contributed to Mabs growth in the airway microenvironment.

***Mycobacterium abscessus* takes advantage of CF-driven oxidative stress to thrive**

As oxidative stress is enhanced in CF AOs, we hypothesised that the CF context could favour Mabs growth. To test this hypothesis, we infected CF-AOs with S- or R-Mabs variant and quantified Mabs proliferation. As shown in Supp Fig. 4A, the S variant formed aggregates whereas the R variant formed cording in CF AOs. At four days post-infection, we observed an enhanced replication of Mabs in CF-AO compared to in H-AOs (Figure 4A-B), indicating that the CF environment favours Mabs fitness. Interestingly, Mabs-infected CF-AOs exhibited more damage in the epithelium than Mabs-infected H-AOs, (Figures 4C-D, Sup Fig. 4B). Next, we used CFTR inhibitors to support our results. CFTR inhibitors by themselves did not alter Mabs growth *in vitro* (Supp Fig. 4C). We treated H-AOs with CFTR inhibitors then infected them with S- and R-Mabs variants and measured bacterial load 4 days post-infection. Treatment of AOs with CFTR inhibitors enhanced Mabs proliferation compared with untreated organoids (Sup Fig. 4D-F), confirming that alteration of CFTR function promoted Mabs growth.

As oxidative stress favoured Mabs growth and CF-AOs displayed increased ROS production, we next evaluated whether antioxidants inhibited Mabs growth. CF-AOs treated with sulforaphane expressed higher NQO-1, confirming Nrf-2 activation (SuppFigure 4G), exhibited mitigated oxidative environment (Figure 4E, Sup Fig. 4G), and reduced bacterial load (Figures 4F-G), indicating that CF-driven oxidative stress stimulated Mabs growth.

Altogether, these results showed that the CF lung environment favoured Mabs fitness, which could be mediated, at least in part, by exuberant oxidative stress due to CFTR dysfunction.

Discussion

In this study, we evaluate the pertinence of CF-patient derived AOs to model CF-associated respiratory infection. We show that AOs derived from a CF patient recapitulate key features of CF disease and that both S- and R-morphotypes of *M. abscessus* proliferate and exhibit infection hallmarks in these AOs. Finally, we demonstrate antioxidant pathways as a potential therapeutic target to better control *Mabs* infection in CF patients. Therefore, AOs derived from CF patients are suitable to model both CF disease and Mabs infection, opening new venues for deciphering critical relevant host pathways and identifying new potential therapeutic intervention.

The organoid technology has demonstrated their usefulness in developing potential therapies for treating CF (51, 52). CF patient-derived organoids bear natural CFTR mutations, thus allowing to recapitulate *ex vivo* the spectrum of CFTR dysfunctions and CF disease severities (30, 53). Extended to the airway, CF patient-derived AOs have been shown to display epithelium hyperplasia, luminal mucus accumulation and abrogated response to forskolin-induced swelling, thus recapitulating CFTR dysfunction and consequences on the airway homeostasis (22). Here, we derived an AO line from a CF patient carrying class I mutations, which lead to the most severe manifestation of CF disease (54). These CF AOs reproduce the expected epithelium hyperplasia, mucus accumulation and defective response to forskolin-induced swelling. Moreover, these CF AOs display enhanced

oxidative stress and lipid peroxidation, as previously measured in CF patients (55, 56) or *in vitro* in CFTR mutated cell lines (57), as well as enhanced cell death recapitulating CF-driven tissue damage. Therefore, AOs derived from CF patients also recapitulate the CF-driven imbalance in oxidant/antioxidant status observed in patients and, importantly, demonstrate that CFTR dysfunction in epithelial cells is sufficient to cause the oxidative status imbalance in the airway epithelium, independent of immune cells.

We and others have already applied the organoid technology to model host-pathogen interactions (22, 24, 25, 29, 58, 59). Here, we have reproduced Mabs infection hallmarks in AOs. Specifically, we show that both S- and R-Mabs replicate in AOs, that S variants are surrounded by an extracellular substance resembling a biofilm, and that the R variant forms serpentine cords associated with higher virulence, in agreement with reported *in vivo* Mabs R hypervirulence compared to Mabs S (5-7). Although Mabs R form characteristic cords *in vitro* and *in vivo* (34, 60), visualizing bacterial biofilm remains a challenge, especially in *ex vivo* and *in vivo* settings. The formation of biofilm plays a crucial role in establishing an infection and at protecting bacilli from immune response and antimicrobial agents, leading to treatment failure (61, 62). Therefore, the detection of biofilm in Mabs S-infected AOs opens new venues to not only testing potential anti-biofilm compounds but also further investigating how the CF lung context favours biofilm formation (61, 63).

ROS production is a part of host antimicrobial defence but requires a fine-tuned balance to prevent tissue damage. Indeed, during Mabs infection, the production of ROS is essential to control infection, as knock-down of NOX2, expressed in immune cells, resulted in uncontrolled bacteria proliferation in zebrafish and mouse models (12, 64). Here, we show that Mabs infection of AOs triggers ROS production through enhanced expression of host ROS production genes NOX1 and DUOX1 concomitantly to enhanced expression of the Nrf2-mediated antioxidant pathway. In alveolar macrophages, Nrf2 deficiency results in a better control of Mtb infection (49), indicating

that early activation of cell protective pathways impairs the control of mycobacteria. By contrast, an oxidative environment has been shown to favour Mabs growth in macrophages (66, 67). Moreover, activation of Nrf2 reduces the bacterial burden both *in vitro* and *in vivo* (47, 48, 50, 68). Finally, apart from its direct antimicrobial effect, the antioxidant N-acetyl cysteine has been shown to inhibit Mtb growth in macrophages and in infected mice (69). Consistently, we show here that treatment of Mabs-infected AOs with resveratrol or sulforaphane results in a better control of bacteria growth. Because resveratrol and sulforaphane do not inhibit Mabs growth *in vitro*, our results indicate that ROS production by epithelial cells is sufficient to generate a permissive environment for Mabs proliferation. Even in the absence of immune cells and low bacteria internalization by epithelial cells (24), AOs recapitulate the contribution of oxidative stress in bacteria fitness in the airway.

Finally, we also show that the enhanced ROS production and the resultant oxidative microenvironment of CF AOs favour the multiplication of Mabs associated with enhanced cell death, recapitulating the higher susceptibility of CF patients to NTM infection (71, 72). Cumulative oxidative stress due to both the CF context and bacterial infection might result in a permissive environment for bacteria growth and the establishment of chronic infection in the lung of CF patients. Interestingly, CF is associated with a defective Nrf2 expression, which contributes to the excessive oxidative stress and lung tissue damage, whereas CFTR modulators rescue Nrf2 function and therefore improve tissue oxidative status (40), which might contribute to a better control of bacterial infection. Here, we show that genetic or pharmacological inhibition of CFTR causes enhanced oxidative stress and bacteria growth, further showing that proper CFTR function in epithelial cells is a part of the intrinsic airway redox balance and homeostasis. CF AOs treated with sulforaphane have reduced oxidative stress and better control of Mabs growth, indicating that activation of Nrf2 can constitute a therapeutic strategy to improve tissue redox homeostasis and

better infection control. Further investigation using animal models are required to integrate ROS production by immune cells. Interestingly, treating R Mabs-infected zebrafishes with resveratrol improves fish survival and reduces bacterial load (48).

A limitation of our study is that only one CF patient-derived organoid line has been used. This CF AO line bears class I mutations that lead to the most severe form of CF disease. As a complementary approach, we also observe better bacteria growth by using CFTR inhibitors to partially alter the CFTR function indicating that this phenotype can also be observed with partially impaired CFTR function as seen with other classes of CFTR mutations. Nevertheless, establishing CF AO lines carrying a wide range of CFTR mutations might be facilitated by emerging protocols (73) and would constitute precious tools to further model the full spectrum of CF disease severity, susceptibility to infection and potential of host-directed therapies targeting oxidative stress on tissue damage (25) and bacteria fitness.

In conclusion, we have established CF patient-derived AOs as a pertinent model of CF airway dysfunction and susceptibility to NTM infection. Moreover, we have identified the cell protective Nrf2 pathway as a potential therapeutic target to restore CF tissue redox homeostasis and improve the control of bacteria growth, opening promising venues to further decipher CF airway dysfunction and susceptibility to infection.

Acknowledgments

We thank Nicole Schieber (EMBL Heidelberg, Germany) for sharing with us the embedding protocol. We thank Veronique Richard and Franck Godiard from the “Microscopie Electronique et Analytique” service of the University of Montpellier for assistance in ultramicrotomy and TEM, respectively. We thank Bruno Payre from the “Centre de Microscopie Electronique pour la Biologie” of the University of Toulouse 3 for his assistance in SEM. This manuscript was edited at Life Science Editors.

References

1. Dechecchi MC, Tamanini A, Cabrini G. Molecular basis of cystic fibrosis: from bench to bedside. *Ann Transl Med* 2018;6:334–334.

2. Lopes-Pacheco M. CFTR Modulators: The Changing Face of Cystic Fibrosis in the Era of Precision Medicine. *Front Pharmacol* 2020;

3. Lopeman RC, Harrison J, Desai M, Cox JAG. Mycobacterium abscessus: Environmental bacterium turned clinical nightmare. *Microorganisms* 2019;7:.

4. Koh WJ, Stout JE, Yew WW. Advances in the management of pulmonary disease due to Mycobacterium abscessus complex. *Int J Tuberc Lung Dis* 2014;

5. Johansen MD, Herrmann J-L, Kremer L. Non-tuberculous mycobacteria and the rise of Mycobacterium abscessus. *Nat Rev Microbiol 2020 187* 2020;18:392–407.

6. Clary G, Sasindran SJ, Nesbitt N, Mason L, Cole S, Azad A, McCoy K, Schlesinger LS, Hall-Stoodley L. Mycobacterium abscessus smooth and rough morphotypes form antimicrobial-tolerant biofilm phenotypes but are killed by acetic acid. *Antimicrob Agents Chemother* 2018;62:.

7. Gutiérrez AV, Viljoen A, Ghigo E, Herrmann J-L, Kremer L. Glycopeptidolipids, a Double-Edged Sword of the Mycobacterium abscessus Complex. *Front Microbiol* 2018;9:1145.

8. To K, Cao R, Yegiazaryan A, Owens J, Venketaraman V. General Overview of Nontuberculous Mycobacteria Opportunistic Pathogens: Mycobacterium avium and Mycobacterium abscessus. *J Clin Med* 2020;9:1–24.

9. Jönsson BE, Gilljam M, Lindblad A, Ridell M, Wold AE, Welinder-Qlsson C. Molecular Epidemiology of Mycobacterium abscessus, with Focus on Cystic Fibrosis. *J Clin Microbiol* 2007;45:1497.

10. Le Moigne V, Raynaud C, Moreau F, Dupont C, Nigou J, Neyrolles O, Kremer L, Herrmann J-L.

Efficacy of bedaquiline, alone or in combination with imipenem, against Mycobacterium abscessus in C3HeB/FeJ mice. *Antimicrob Agents Chemother* 2020;doi:10.1128/AAC.00114-20.

11. Bernut A, Le Moigne V, Lesne T, Lutfalla G, Herrmann JL, Kremer L. In Vivo assessment of drug efficacy against Mycobacterium abscessus using the embryonic zebrafish test system. *Antimicrob Agents Chemother* 2014;58:4054–4063.

12. Bernut A, Dupont C, Ogryzko N V., Neyret A, Herrmann JL, Floto RA, Renshaw SA, Kremer L. CFTR Protects against Mycobacterium abscessus Infection by Fine-Tuning Host Oxidative Defenses. *Cell Rep* 2019;26:1828-1840.e4.

13. Lefebvre AL, Le Moigne V, Bernut A, Veckerlé C, Compain F, Herrmann JL, Kremer L, Arthur M, Mainardi JL. Inhibition of the β-lactamase BlaMab by avibactam improves the in vitro and in vivo efficacy of imipenem against Mycobacterium abscessus. *Antimicrob Agents Chemother* 2017;61:.

14. Lopez A, Shoen C, Cynamon M, Dimitrakopoulou D, Paiola M, Pavelka MS, Robert J. Developing tadpole xenopus laevis as a comparative animal model to study Mycobacterium abscessus pathogenicity. *Int J Mol Sci* 2021;22:1–12.

15. Bernut A, Herrmann J-L, Ordway D, Kremer L. The Diverse Cellular and Animal Models to Decipher the Physiopathological Traits of Mycobacterium abscessus Infection. *Front Cell Infect Microbiol* 2017;7:100.

16. McCarron A, Parsons D, Donnelley M. Animal and Cell Culture Models for Cystic Fibrosis: Which Model Is Right for Your Application? *Am J Pathol* 2021;191:228–242.

17. McCarron A, Donnelley M, Parsons D. Airway disease phenotypes in animal models of cystic fibrosis. *Respir Res* 2018;19:1–12.

18. Semaniakou A, Croll RP, Chappe V. Animal Models in the Pathophysiology of Cystic Fibrosis.

Front Pharmacol 2018;9:.

19. Schutgens F, Clevers H. Human Organoids: Tools for Understanding Biology and Treating Diseases. *Annu Rev Pathol* 2020;15:211–234.

20. Kim J, Koo BK, Knoblich JA. Human organoids: model systems for human biology and medicine. *Nat Rev Mol Cell Biol 2020 2110* 2020;21:571–584.

21. Clevers H. Modeling Development and Disease with Organoids. *Cell* 2016;165:1586–1597.

22. Sachs N, Papaspyropoulos A, Zomer-van Ommen DD, Heo I, Böttinger L, Klay D, Weeber F, Huelsz-Prince G, Iakobachvili N, Amatngalim GD, Ligt J, Hoeck A, Proost N, Viveen MC, Lyubimova A, Teeven L, Derakhshan S, Korving J, Begthel H, Dekkers JF, Kumawat K, Ramos E, Oosterhout MF, Offerhaus GJ, Wiener DJ, Olimpio EP, Dijkstra KK, Smit EF, Linden M, *et al.* Long-term expanding human airway organoids for disease modeling. *EMBO J* 2019;38:.

23. Iakobachvili N, Peters PJ. Humans in a dish: The potential of organoids in modeling immunity and infectious diseases. *Front Microbiol* 2017;8:.

24. Iakobachvili N, Leon-Icaza SA, Knoops K, Sachs N, Mazères S, Simeone R, Peixoto A, Bernard C, Murris-Espin M, Mazières J, Cam K, Chalut C, Guilhot C, López-Iglesias C, Ravelli RBG, Neyrolles O, Meunier E, Lugo-Villarino G, Clevers H, Cougoule C, Peters PJ. Mycobacteria-host interactions in human bronchiolar airway organoids. *Mol Microbiol* 2021;00:1–11.

25. Bagayoko S, Leon-Icaza SA, Pinilla M, Hessel A, Santoni K, Péricat D, Bordignon PJ, Moreau F, Eren E, Boyancé A, Naser E, Lefèvre L, Berrone C, Iakobachvili N, Metais A, Rombouts Y, Lugo-Villarino G, Coste A, Attrée I, Frank DW, Clevers H, Peters PJ, Cougoule C, Planès R, Meunier E. Host phospholipid peroxidation fuels ExoU-dependent cell necrosis and supports Pseudomonas aeruginosa-driven pathology. *PLoS Pathog* 2021;17:.

26. Kronemberger GS, Carneiro FA, Rezende DF, Baptista LS. Spheroids and organoids as humanized 3D scaffold-free engineered tissues for SARS-CoV-2 viral infection and drug

screening. *Artif Organs* 2021;doi:10.1111/aor.13880.

27. Mykytyn AZ, Breugem TI, Riesebosch S, Schipper D, van den Doel PB, Rottier RJ, Lamers MM, Haagmans BL. Sars-cov-2 entry into human airway organoids is serine protease-mediated and facilitated by the multibasic cleavage site. *Elife* 2021;10:1–23.

28. Han Y, Duan X, Yang L, Nilsson-Payant BE, Wang P, Duan F, Tang X, Yaron TM, Zhang T, Uhl S, Bram Y, Richardson C, Zhu J, Zhao Z, Redmond D, Houghton S, Nguyen DHT, Xu D, Wang X, Jessurun J, Borczuk A, Huang Y, Johnson JL, Liu Y, Xiang J, Wang H, Cantley LC, tenOever BR, Ho DD, *et al.* Identification of SARS-CoV-2 inhibitors using lung and colonic organoids. *Nature* 2021;589:270–275.

29. Heo I, Dutta D, Schaefer DA, Iakobachvili N, Artegiani B, Sachs N, Boonekamp KE, Bowden G, Hendrickx APA, Willems RJL, Peters PJ, Riggs MW, O'Connor R, Clevers H. Modelling Cryptosporidium infection in human small intestinal and lung organoids. *Nat Microbiol* 2018;3:814–823.

30. de Winter – de Groot KM, Berkers G, Marck – van der Wilt REP, van der Meer R, Vonk A, Dekkers JF, Geerdink M, Michel S, Kruisselbrink E, Vries R, Clevers H, Vleggaar FP, Elias SG, Heijerman HGM, van der Ent CK, Beekman JM. Forskolin-induced swelling of intestinal organoids correlates with disease severity in adults with cystic fibrosis and homozygous F508del mutations. *J Cyst Fibros* 2020;19:614–619.

31. Dekkers JF, Berkers G, Kruisselbrink E, Vonk A, De Jonge HR, Janssens HM, Bronsveld I, Van De Graaf EA, Nieuwenhuis EES, Houwen RHJ, Vleggaar FP, Escher JC, De Rijke YB, Majoor CJ, Heijerman HGM, De Winter-De Groot KM, Clevers H, Van Der Ent CK, Beekman JM. Characterizing responses to CFTR-modulating drugs using rectal organoids derived from subjects with cystic fibrosis. *Sci Transl Med* 2016;8:344ra84-344ra84.

32. Bartfeld S, Clevers H. Organoids as model for infectious diseases: Culture of human and

murine stomach organoids and microinjection of helicobacter pylori. *J Vis Exp* 2015;2015:.

33. Boj SF, Vonk AM, Statia M, Su J, Vries RRG, Beekman JM, Clevers H. Forskolin-induced Swelling in Intestinal Organoids: An In Vitro Assay for Assessing Drug Response in Cystic Fibrosis Patients. *J Vis Exp* 2017;2017:.

34. Bernut A, Herrmann JL, Kissa K, Dubremetz JF, Gaillard JL, Lutfalla G, Kremer L. Mycobacterium abscessus cording prevents phagocytosis and promotes abscess formation. *Proc Natl Acad Sci U S A* 2014;111:E943–E952.

35. Lastrucci C, Bénard A, Balboa L, Pingris K, Souriant S, Poincloux R, Al Saati T, Rasolofo V, González-Montaner P, Inwentarz S, Moraña EJ, Kondova I, Verreck FAW, Del Carmen Sasiain M, Neyrolles O, Maridonneau-Parini I, Lugo-Villarino G, Cougoule C. Tuberculosis is associated with expansion of a motile, permissive and immunomodulatory CD16(+) monocyte population via the IL-10/STAT3 axis. *Cell Res* 2015;25:1333–1351.

36. Shteinberg M, Haq IJ, Polineni D, Davies JC. Cystic fibrosis. *Lancet* 2021;397:2195–2211.

37. Ghigo A, Prono G, Riccardi E, De Rose V. Dysfunctional Inflammation in Cystic Fibrosis Airways: From Mechanisms to Novel Therapeutic Approaches. *Int J Mol Sci* 2021;22:1–23.

38. Chen J, Kinter M, Shank S, Cotton C, Kelley TJ, Ziady AG. Dysfunction of Nrf-2 in CF epithelia leads to excess intracellular H2O2 and inflammatory cytokine production. *PLoS One* 2008;3:.

39. Galli F, Battistoni A, Gambari R, Pompella A, Bragonzi A, Pilolli F, Iuliano L, Piroddi M, Dechecchi MC, Cabrini G. Oxidative stress and antioxidant therapy in cystic fibrosis. *Biochim Biophys Acta - Mol Basis Dis* 2012;

40. Borcherding DC, Siefert ME, Lin S, Brewington J, Sadek H, Clancy JP, Plafker SM, Ziady AG. Clinically approved CFTR modulators rescue Nrf2 dysfunction in cystic fibrosis airway epithelia. *J Clin Invest* 2019;129:3448–3463.

41. Koch RE, Hill GE. An assessment of techniques to manipulate oxidative stress in animals.

Funct Ecol 2017;31:9–21.

42. Benabdeslam H, Abidi H, Garcia I, Bellon G, Gilly R, Revol A. Lipid peroxidation and antioxidant defenses in cystic fibrosis patients. *Clin Chem Lab Med* 1999;37:511–516.

43. Su LJ, Zhang JH, Gomez H, Murugan R, Hong X, Xu D, Jiang F, Peng ZY. Reactive Oxygen Species-Induced Lipid Peroxidation in Apoptosis, Autophagy, and Ferroptosis. *Oxid Med Cell Longev* 2019;2019:.

44. Juan CA, de la Lastra JMP, Plou FJ, Pérez-Lebeña E. The Chemistry of Reactive Oxygen Species (ROS) Revisited: Outlining Their Role in Biological Macromolecules (DNA, Lipids and Proteins) and Induced Pathologies. *Int J Mol Sci* 2021;22:4642.

45. Davidson LB, Nessar R, Kempaiah P, Perkins DJ, Byrd TF. Mycobacterium abscessus Glycopeptidolipid Prevents Respiratory Epithelial TLR2 Signaling as Measured by HβD2 Gene Expression and IL-8 Release. In: Fessler MB, editor. *PLoS One* 2011;6:e29148.

46. McCutcheon J, Southam G. Advanced biofilm staining techniques for TEM and SEM in geomicrobiology: Implications for visualizing EPS architecture, mineral nucleation, and microfossil generation. *Chem Geol* 2018;498:115–127.

47. Bonay M, Roux AL, Floquet J, Retory Y, Herrmann JL, Lofaso F, Deramaudt T. Caspase-independent apoptosis in infected macrophages triggered by sulforaphane via Nrf2/p38 signaling pathways. *Cell Death Discov* 2015;1:1.

48. Kim YJ, Lee SH, Jeon SM, Silwal P, Seo JY, Hanh BTB, Park JW, Whang J, Lee MJ, Heo JY, Kim SH, Kim JM, Song GY, Jang J, Jo EK. Sirtuin 3 is essential for host defense against Mycobacterium abscessus infection through regulation of mitochondrial homeostasis. *Virulence* 2020;11:1225–1239.

49. Rothchild AC, Olson GS, Nemeth J, Amon LM, Mai D, Gold ES, Diercks AH, Aderem A. Alveolar macrophages generate a noncanonical NRF2-driven transcriptional response to

Mycobacterium tuberculosis in vivo. *Sci Immunol* 2019;4:.

50. Nakajima M, Matsuyama M, Kawaguchi M, Kiwamoto T, Matsuno Y, Morishima Y, Yoshida K, Sherpa M, Yazaki K, Osawa H, Muratani M, Ishii Y, Hizawa N. Nrf2 regulates granuloma formation and macrophage activation during mycobacterium avium infection via mediating nramp1 and ho-1 expressions. *MBio* 2021;12:1–17.

51. Graeber SY, van Mourik P, Vonk AM, Kruisselbrink E, Hirtz S, van der Ent CK, Mall MA, Beekman JM. Comparison of Organoid Swelling and In Vivo Biomarkers of CFTR Function to Determine Effects of Lumacaftor-Ivacaftor in Patients with Cystic Fibrosis Homozygous for the F508del Mutation. *Am J Respir Crit Care Med* 2020;202:1589–1592.

52. Anderson JD, Liu Z, Odom LV, Kersh L, Guimbellot JS. CFTR function and clinical response to modulators parallel nasal epithelial organoid swelling. *Am J Physiol Lung Cell Mol Physiol* 2021;321:L119–L129.

53. de Winter-De Groot KM, Janssens HM, van Uum RT, Dekkers JF, Berkers G, Vonk A, Kruisselbrink E, Oppelaar H, Vries R, Clevers H, Houwen RHJ, Escher JC, Elias SG, De Jonge HR, de Rijke YB, Tiddens HAWM, van der Ent CK, Beekman JM. Stratifying infants with cystic fibrosis for disease severity using intestinal organoid swelling as a biomarker of CFTR function. *Eur Respir J* 2018;52:.

54. Reboul MP, Bieth E, Fayon M, Biteau N, Barbier R, Dromer C, Desgeorges M, Claustres M, Bremont F, Lacombe D, Iron A. Splice mutation 1811+1.6kbA>G causes severe cystic fibrosis with pancreatic insufficiency: report of 11 compound heterozygous and two homozygous patients. *J Med Genet* 2002;39:.

55. Winklhofer-Roob BM. Oxygen free radicals and antioxidants in cystic fibrosis: the concept of an oxidant-antioxidant imbalance. *Acta Paediatr Suppl* 1994;83:49–57.

56. Causer AJ, Shute JK, Cummings MH, Shepherd AI, Gruet M, Costello JT, Bailey S, Lindley M,

Pearson C, Connett G, Allenby MI, Carroll MP, Daniels T, Saynor ZL. Circulating biomarkers of antioxidant status and oxidative stress in people with cystic fibrosis: A systematic review and meta-analysis. *Redox Biol* 2020;32:.

57. de Bari L, Favia M, Bobba A, Lassandro R, Guerra L, Atlante A. Aberrant GSH reductase and NOX activities concur with defective CFTR to pro-oxidative imbalance in cystic fibrosis airways. *J Bioenerg Biomembr* 2018;50:117–129.

58. Lamers MM, van der Vaart J, evin Knoops K, Riesebosch S, Breugem TI, Mykytyn AZ, Beumer J, Schipper D, Bezstarosti K, Koopman CD, Groen N, G Ravelli RB, Duimel HQ, A Demmers JA, G M Verjans GM, G Koopmans MP, Muraro MJ, Peters PJ, Clevers H, Haagmans BL. An organoid-derived bronchioalveolar model for SARS-CoV-2 infection of human alveolar type II-like cells. *EMBO J* 2021;40:e105912.

59. Zhou J, Li C, Sachs N, Chiu MC, Wong BHY, Chu H, Poon VKM, Wang D, Zhao X, Wen L, Song W, Yuan S, Wong KKY, Chan JFW, To KKW, Chen H, Clevers H, Yuen KY. Differentiated human airway organoids to assess infectivity of emerging influenza virus. *Proc Natl Acad Sci U S A* 2018;115:6822–6827.

60. Roux AL, Viljoen A, Bah A, Simeone R, Bernut A, Laencina L, Deramaudt T, Rottman M, Gaillard JL, Majlessi L, Brosch R, Girard-Misguich F, Vergne I, de Chastellier C, Kremer L, Herrmann JL. The distinct fate of smooth and rough Mycobacterium abscessus variants inside macrophages. *Open Biol* 2016;6:.

61. Chakraborty P, Bajeli S, Kaushal D, Radotra BD, Kumar A. Biofilm formation in the lung contributes to virulence and drug tolerance of Mycobacterium tuberculosis. *Nat Commun* 2021;12:.

62. Esteban J, García-Coca M. Mycobacterium Biofilms. *Front Microbiol* 2018;8:.

63. Bjarnsholt T. The role of bacterial biofilms in chronic infections. *APMIS Suppl* 2013;1–

51.doi:10.1111/APM.12099.

64. Chao WC, Yen CL, Hsieh CY, Huang YF, Tseng YL, Nigrovic PA, Shieh CC. Mycobacterial infection induces higher interleukin-1β and dysregulated lung inflammation in mice with defective leukocyte NADPH oxidase. *PLoS One* 2017;12:.

65. Abdalla MY, Ahmad IM, Switzer B, Britigan BE. Induction of heme oxygenase-1 contributes to survival of Mycobacterium abscessus in human macrophages-like THP-1 cells. *Redox Biol* 2015;4:328–339.

66. Kim BR, Kim BJ, Kook YH, Kim BJ. Mycobacterium abscessus infection leads to enhanced production of type 1 interferon and NLRP3 inflammasome activation in murine macrophages via mitochondrial oxidative stress. *PLoS Pathog* 2020;16:.

67. Oberley-Deegan RE, Rebits BW, Weaver MR, Tollefson AK, Bai X, McGibney M, Ovrutsky AR, Chan ED, Crapo JD. An oxidative environment promotes growth of Mycobacterium abscessus. *Free Radic Biol Med* 2010;49:1666–1673.

68. Sun Q, Shen X, Ma J, Lou H, Zhang Q. Activation of Nrf2 signaling by oltipraz inhibits death of human macrophages with mycobacterium tuberculosis infection. *Biochem Biophys Res Commun* 2020;531:312–319.

69. Amaral EP, Conceição EL, Costa DL, Rocha MS, Marinho JM, Cordeiro-Santos M, D'Império-Lima MR, Barbosa T, Sher A, Andrade BB. N-acetyl-cysteine exhibits potent anti-mycobacterial activity in addition to its known anti-oxidative functions. *BMC Microbiol* 2016;16:1–10.

70. Ross D, Siegel D. Functions of NQO1 in cellular protection and CoQ10 metabolism and its potential role as a redox sensitive molecular switch. *Front Physiol* 2017;8:595.

71. Furukawa BS, Flume PA. Nontuberculous Mycobacteria in Cystic Fibrosis. *Semin Respir Crit Care Med* 2018;39:383–391.

72. Qvist T, Taylor-Robinson D, Waldmann E, Olesen HV, Hansen CR, Mathiesen IH, Høiby N, Katzenstein TL, Smyth RL, Diggle PJ, Pressler T. Comparing the harmful effects of nontuberculous mycobacteria and Gram negative bacteria on lung function in patients with cystic fibrosis. *J Cyst Fibros* 2016;15:380–385.

73. van der Vaart J., Böttinger L., Geurts M.H., van de Wetering W.J., Knoops K., Sachs N., Begthel H., Korving J., Lopez Iglesias C., Peters P.J., Eitan K., Gileles-Hillel A., Clevers H. Modelling of primary ciliary dyskinesia using patient-derived airway organoids. *EMBO Rep*. 2021; 6;22(12):e52058.

Figure legends

Figure 1. Patient-derived airway organoids recapitulate Cystic fibrosis-driven oxidative stress. (A, B) Representative bright-field images (A) and quantification (B) of epithelium thickness in healthy AOs (H-AO, n=32) and cystic fibrosis AOs (CF-AO, n=24) after 5 weeks of growing. Data from three independent wells per donor. (C) Percentage of area increase of H-AO (n=13), H-AO pre-treated with CFTR inhibitors for 4 days (CFTR-Inh, n=13), and CF-AO (n=13) after 2hr stimulation with 5µM forskolin. Data from two independent wells per donor. (D, E) Representative images (D) and Mean Fluorescence Intensity (MFI) quantification (E) of mucus staining (Zinpyr-1) in H-AO (n=10) and CF-AO (n=8). (F) The volcano plot showing the fold-change (x-axis) versus the significance (y-axis) of the proteins identified by LC–MS/MS in CF-AOs vs in H-AOs. The significance (non-adjusted p-value) and the fold-change are converted to −Log10(p-value) and Log2(fold-change), respectively. (G, H) Representative images (G) and MFI quantification (H) of basal mitochondrial ROS production (MitoSOX) in H-AO (n=6) and CF-AO (n=6). (I) MFI quantification of basal H_2O_2 production (H2DCFDA) in H-AO (n=12) and CF-AO (n=22). (J, K) Representative images (J) and MFI quantification (K) of peroxidized lipids (BODIPY) in H-AO (n=14) and CF-AO (n=14). (L) MFI quantification of the basal

plasma membrane permeabilization (propidium iodide incorporation) in H-AO (n=6) and CF-AO (n=6). Except otherwise noted, graphs represent means ± SD from at least two independent experiments indicated by different symbols. Each dot represents one organoid. *P<0.05; **P<0.01; ***P<0.001, **** P<0.0001 by Mann-Whitney test.

Figure 2. Mabs infection in healthy airway organoids. (A) Kinetics of Mabs S and R growth in H-AO. Graph shows three pooled independent experiments. (B) Representative images of Mock (PBS) infected H-AO or H-AO infected with tdTomato-labelled Mabs S or R. (C) Light-sheet fluorescence microscopy of a XY plane at the z=120µm (left two images) or z=80µm (right two images) positions of a H-AO infected with Mabs S and R, respectively; Zoom-in image of the yellow square zone. (D) Electron micrographs obtained with a FEI Quanta200 scanning electron microscope set up in back-scattered mode. Resin blocks were sectioned and imaged at different magnifications showing normal H-AO organization and the different cell types typical of lung epithelium (top row), the biofilm formed by Mabs S on the luminal face of the epithelial cells (middle row), and the bacterial aggregates typical of the cording in the lumen of Mabs R infected H-AO (bottom row). Targeted ultrathin sections were made and observed by transmission electron microscopy (images 5 and 8). (E, F) Representative images (E) and MFI quantification (F) of propidium iodide incorporation in Mock infected H-AOs (n=13) or H-AOs infected with Wasabi-labelled Mabs S (n=17) or R (n=15) for 4 days. The dotted lines delimit the organoids circumference. Graph represents means ± SD from three independent experiments, indicated by different symbols. Each dot represents one organoid. *P<0.05; **P<0.01; ***P<0.001 by Mann-Whitney test. Yellow boxes in figure 2B and 2E indicate inset area and scale bars represent 10µm.

Figure 3. Mabs promote an oxidative environment in healthy airway organoids. (A) Heatmap depicting ROS-related genes in Mock-infected H-AO or H-AO infected with Mabs S or R for 4 days. Heatmap represents means from three pooled independent experiments, performed in triplicates.

*P<0.05; ***P<0.001 by unpaired T test. (B, C) Representative images (B) and MFI quantification (C) of mitochondrial ROS production (MitoSOX) in Mock-infected H-AOs (n=17) or H-AO infected with Wasabi-labelled Mabs S (n=13) or R (n=8) for 3 days. (D) MFI quantification of H_2O_2 production (H2DCFDA) in Mock-infected H-AOs (n=7) or H-AO infected with tdTomato-labelled Mabs S (n=7) or R (n=7) for 3 days. (E-F) Bacterial load by CFU assay of H-AOs pre-treated with (+) or without (-) resveratrol for 1hr before infection with Mabs S (E) (n+= 7; n-=6) or R (F) (n+= 8; n-=6) for 4 days. (G-H) Bacterial load by CFU assay of H-AO pre-treated with (+) or without (-) sulforaphane for 6hr before infection with Mabs S (G) (n+= 8; n-=8) or R (H) (n+= 9; n-=9) for 4 days. Except otherwise stated, graphs represent means ± SD from at least two independent experiments, indicated by different symbols. Each dot represents one organoid. *P<0.05; **P<0.01; ***P<0.001, **** P<0.0001 by Mann-Whitney test.

Figure 4. Oxidative stress in cystic fibrosis benefits Mabs growth. (A-B) Bacterial load by CFU assay of H-AO and CF-AO infected for 4 days with Mabs S (A) (n healthy=11; n cystic fibrosis=15) or R (B) (n healthy=10; n cystic fibrosis=13). (C, D) Representative images (C) and MFI quantification (D) of propidium iodide incorporation in Mock-infected H-AO and CF-AO (n healthy= 9; n cystic fibrosis= 10) or H-AO and CF-AO infected with Wasabi-labelled Mabs S (n healthy= 6; n cystic fibrosis= 6) or R (n healthy= 7; n cystic fibrosis= 6) for 4 days. (E) MFI quantification of mitochondrial ROS production (MitoSOX) in H-AO (n=10) and CF-AO (n+=12; n-=12) after 4 days of being treated with (+) or without (-) sulforaphane. (F-G) Bacterial load by CFU assay of CF-AO pre-treated with (+) or without (-)sulforaphane for 6 hr before infection with Mabs S (G) (n+= 7; n-=8) or R (H) (n+= 7; n-=6) for 4 days. Except otherwise stated, graphs represent means ± SD from at least two independent experiments, indicate them by different symbols. Each dot represents one organoid. *P<0.05; **P<0.01; **** P<0.0001 by Mann-Whitney test.

Figure 1

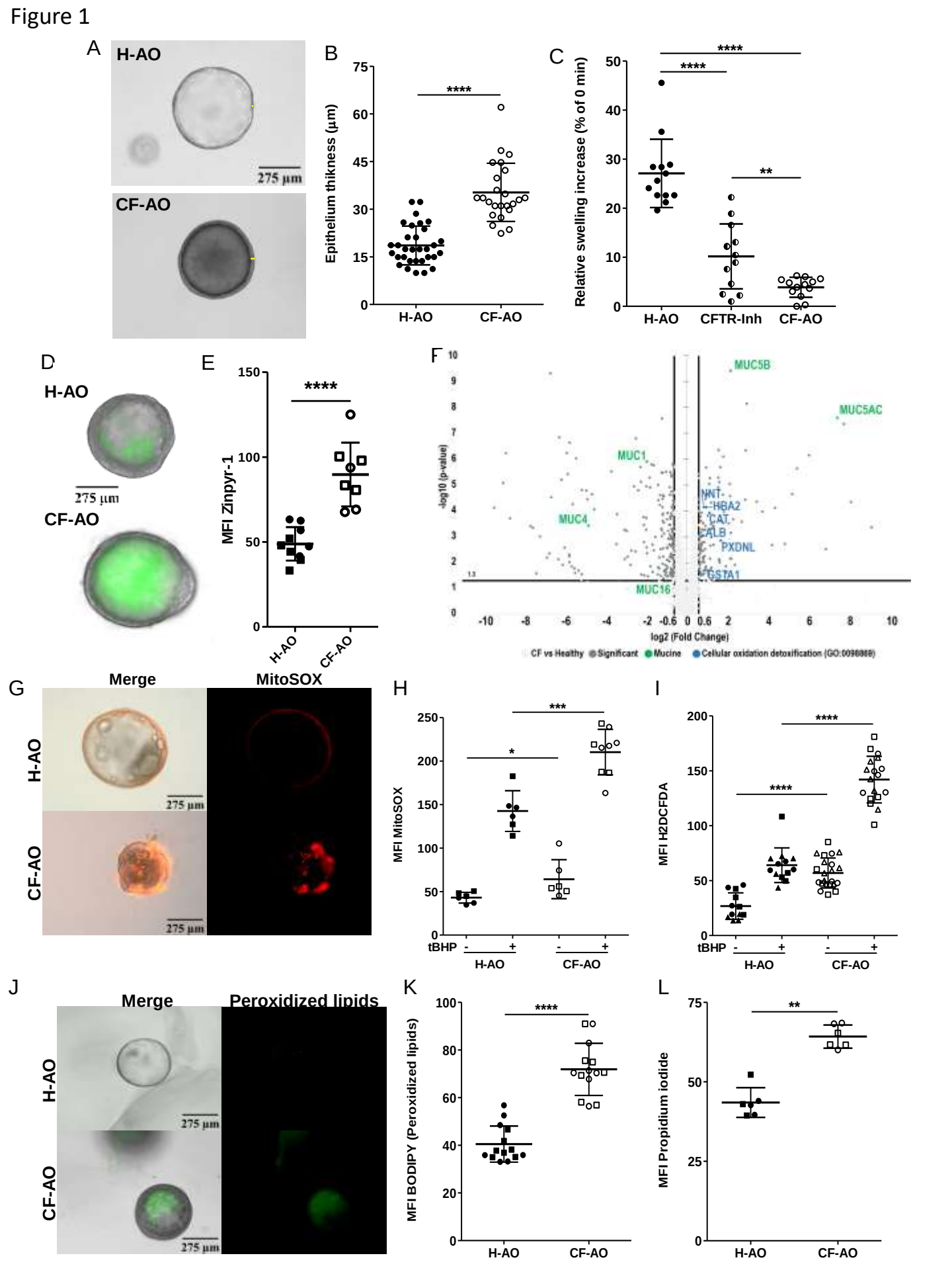
A
H-AO
275 µm
CF-AO
B
Epithelium thikness (µm)
H-AO
CF-AO
C
Relative swelling increase (% of 0 min)
H-AO
CFTR-Inh
CF-AO
D
H-AO
275 µm
CF-AO
E
MFI Zinpyr-1
H-AO
CF-AO
F
MUC5B
MUC5AC
MUC1
MUC4
MUC16
-log10 (p-value)
log2 (Fold Change)
CF vs Healthy
Significant
Mucins
Cellular oxidation detoxification (GO:0098869)
G
Merge
MitoSOX
H-AO
CF-AO
H
MFI MitoSOX
tBHP
H-AO
CF-AO
I
MFI H2DCFDA
tBHP
H-AO
CF-AO
J
Merge
Peroxidized lipids
H-AO
CF-AO
K
MFI BODIPY (Peroxidized lipids)
H-AO
CF-AO
L
MFI Propidium iodide
H-AO
CF-AO

Figure 2

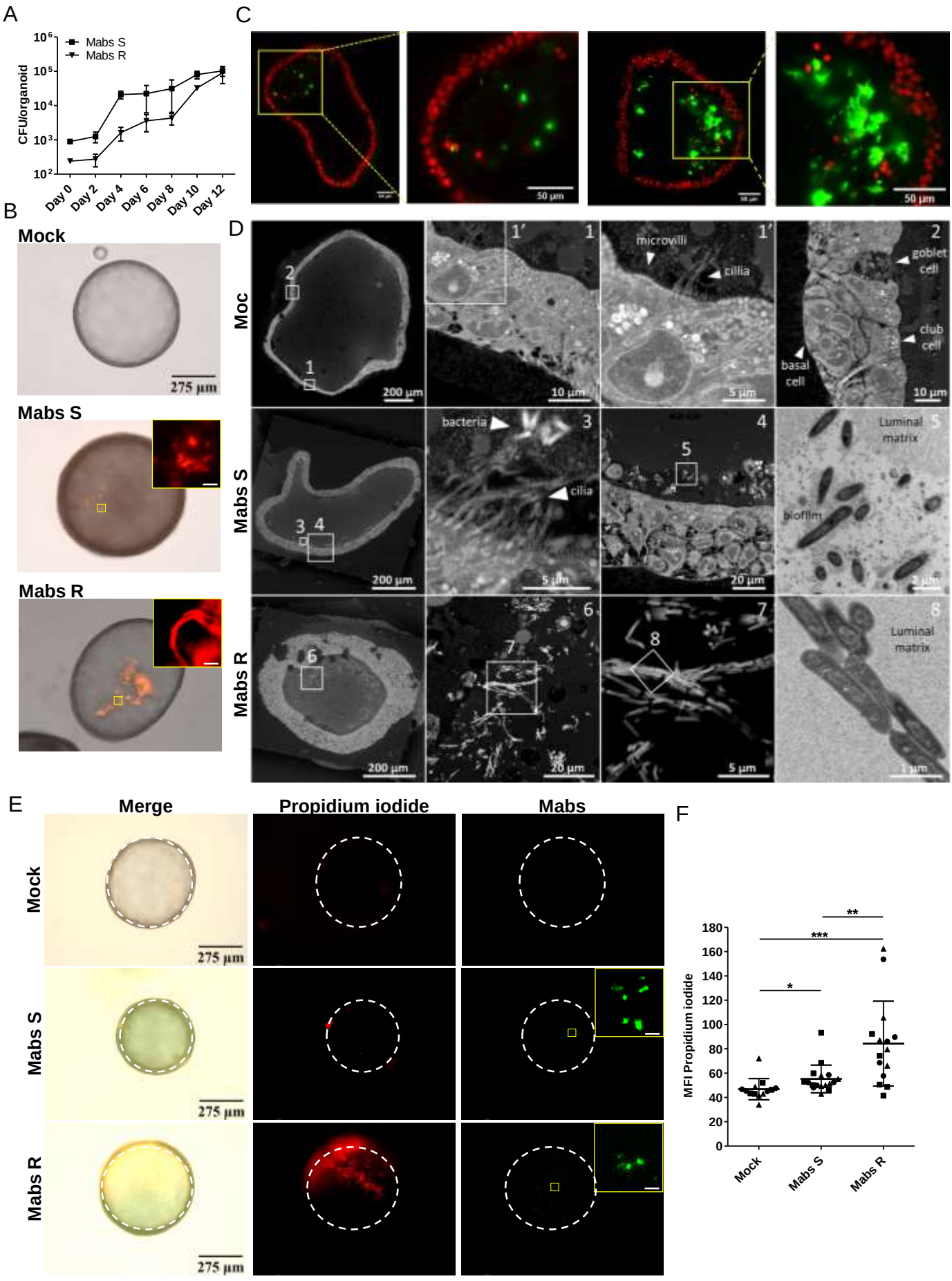
A
Mabs S
Mabs R
CFU/organoid
Day 0
Day 2
Day 4
Day 6
Day 8
Day 10
Day 12
B
Mock
Mabs S
Mabs R
275 µm
C
50 µm
D
Moc
Mabs S
Mabs R
microvilli
cillia
goblet cell
club cell
basal cell
bacteria
cilia
Luminal matrix
biofilm
200 µm
10 µm
5 µm
20 µm
1 µm
E
Merge
Propidium iodide
Mabs
Mock
Mabs S
Mabs R
275 µm
F
MFI Propidium iodide
Mock
Mabs S
Mabs R

Figure 3

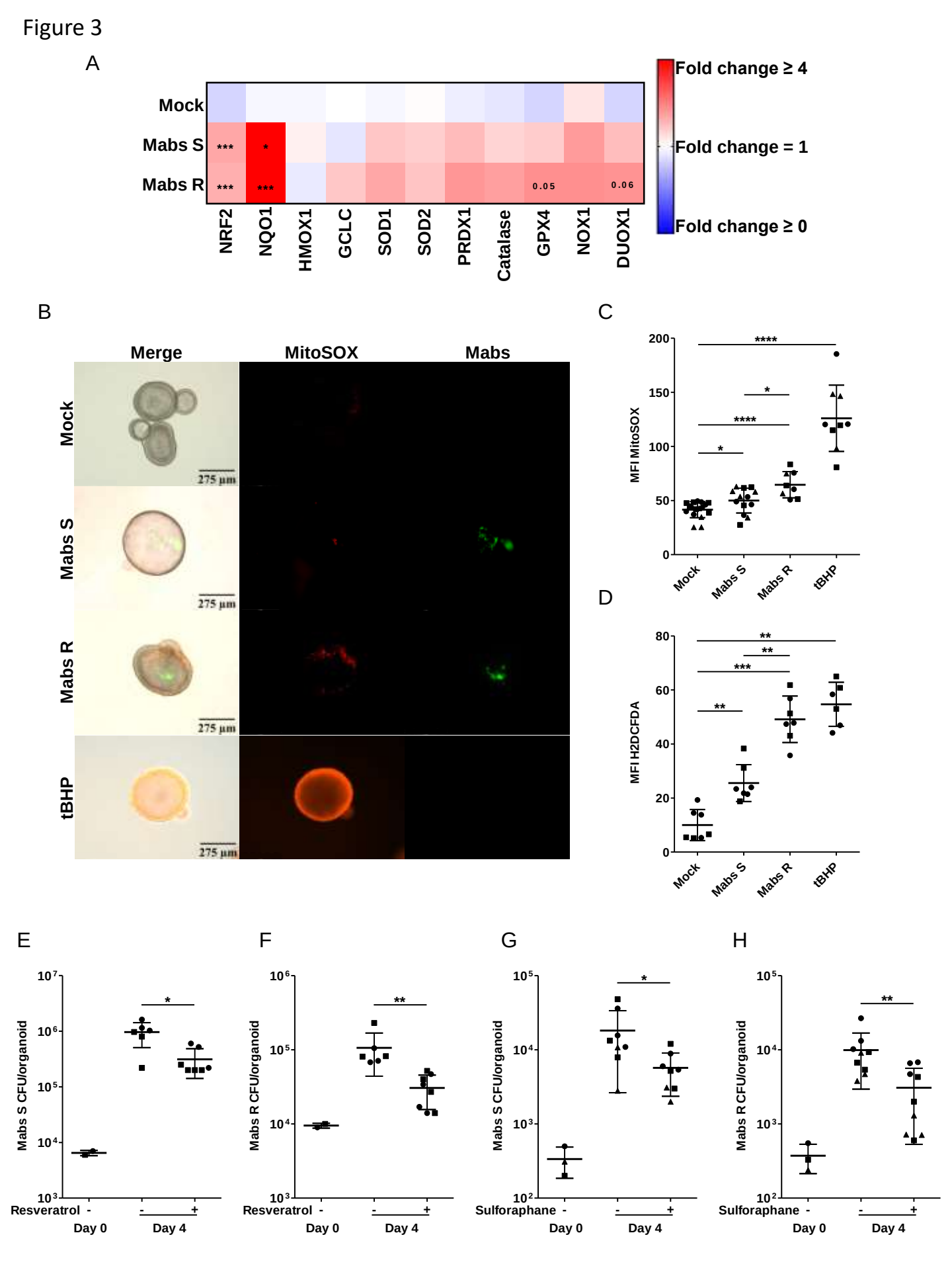
A
Mock
Mabs S
Mabs R
NRF2
NQO1
HMOX1
GCLC
SOD1
SOD2
PRDX1
Catalase
GPX4
NOX1
DUOX1
Fold change ≥ 4
Fold change = 1
Fold change ≥ 0
B
Merge
MitoSOX
Mabs
Mock
Mabs S
Mabs R
tBHP
275 µm
C
MFI MitoSOX
D
MFI H2DCFDA
E
Mabs S CFU/organoid
Resveratrol
Day 0
Day 4
F
Mabs R CFU/organoid
G
Sulforaphane
H

Figure 4

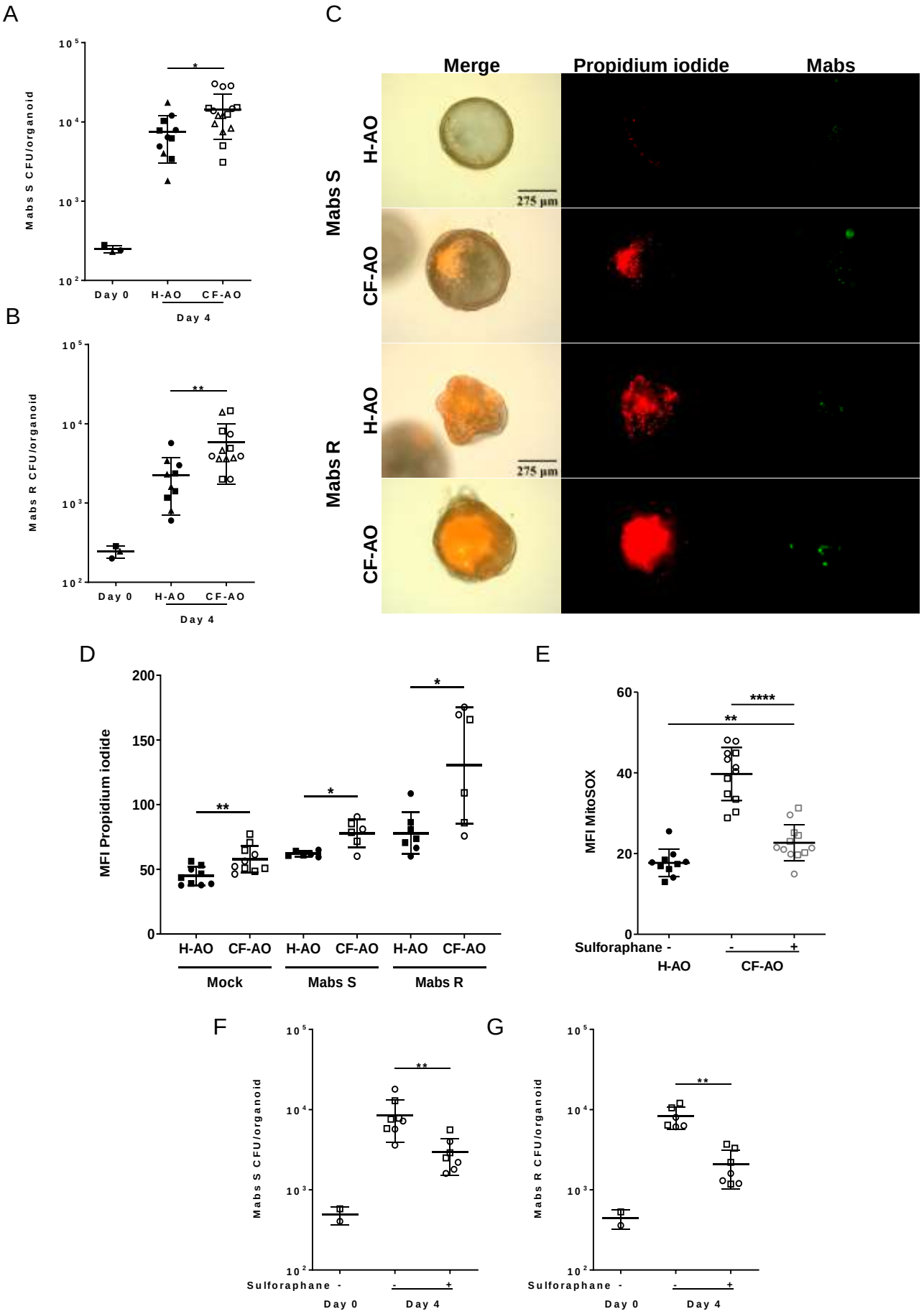
A
Mabs S CFU/organoid
Day 0
H-AO
CF-AO
Day 4
B
Mabs R CFU/organoid
C
Merge
Propidium iodide
Mabs
Mabs S
Mabs R
H-AO
CF-AO
275 µm
D
MFI Propidium iodide
Mock
Mabs S
Mabs R
E
MFI MitoSOX
Sulforaphane -
+
F
G

Supp Figure 1

A

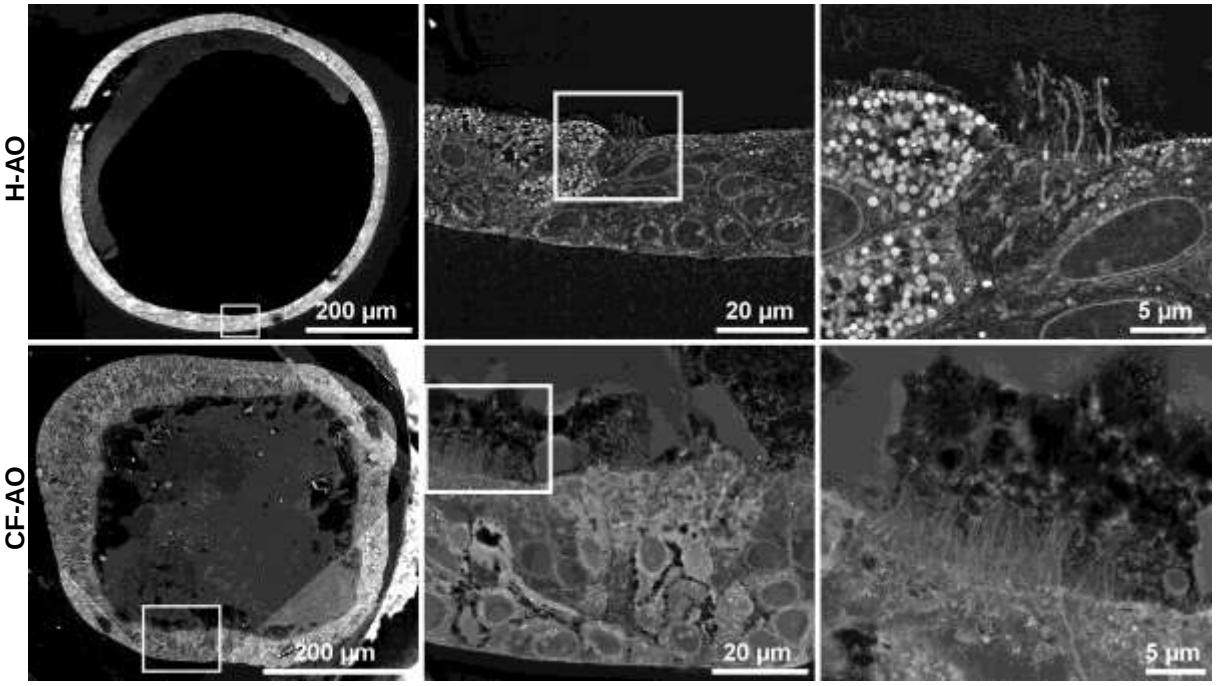

B

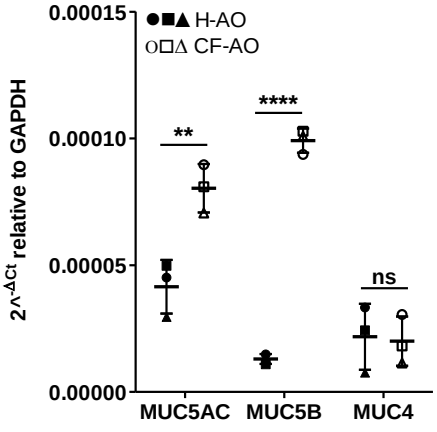

C

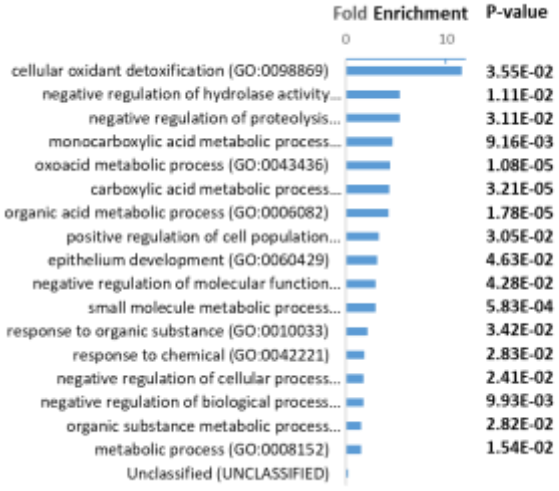

D

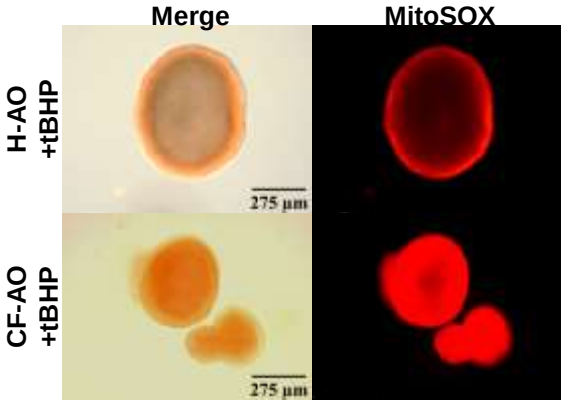

E

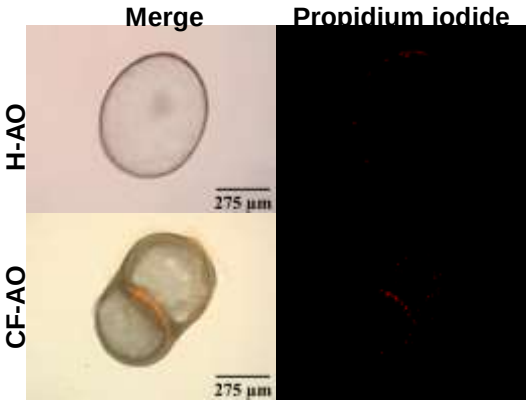

Supp Figure 2

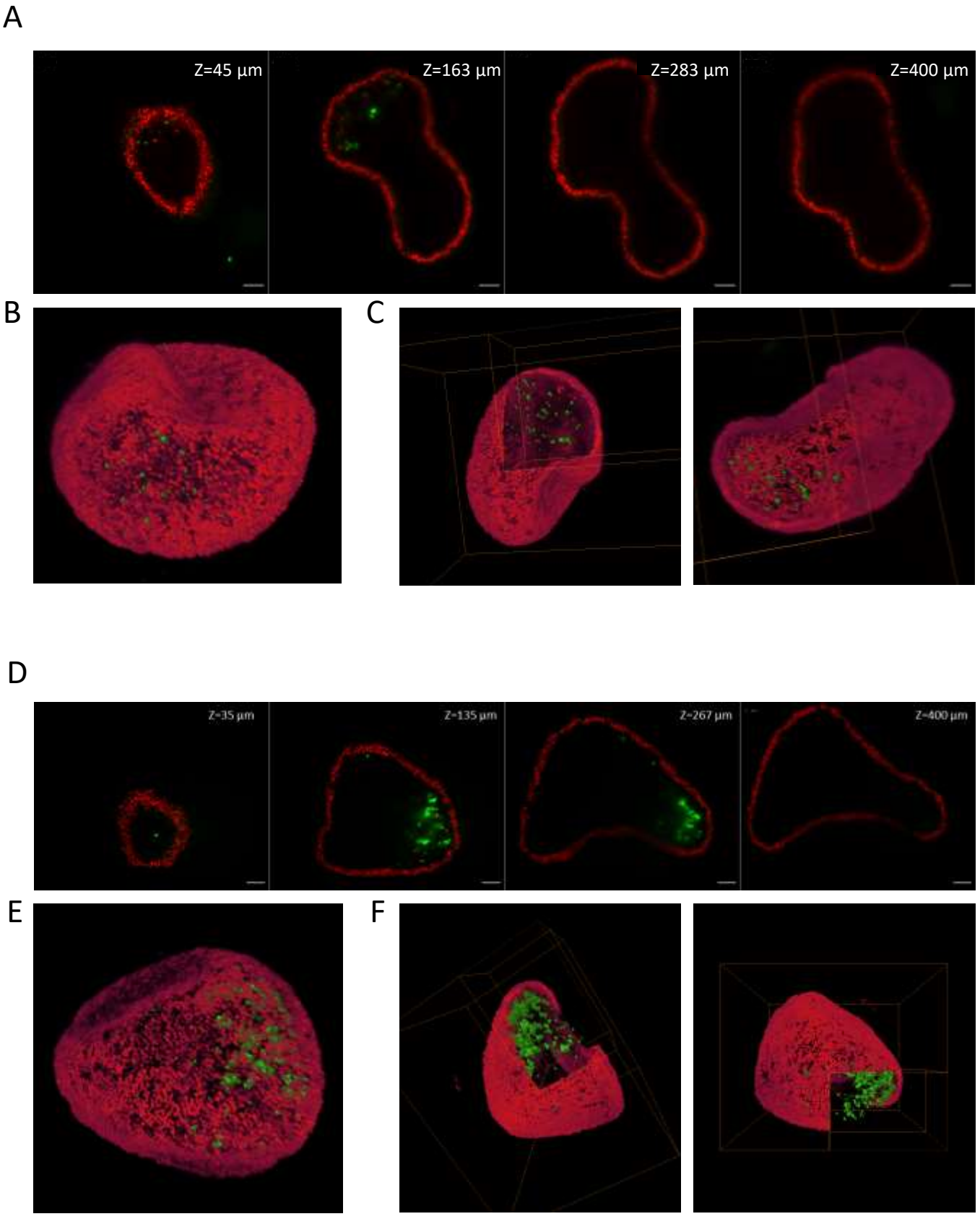

Supp Figure 3

A

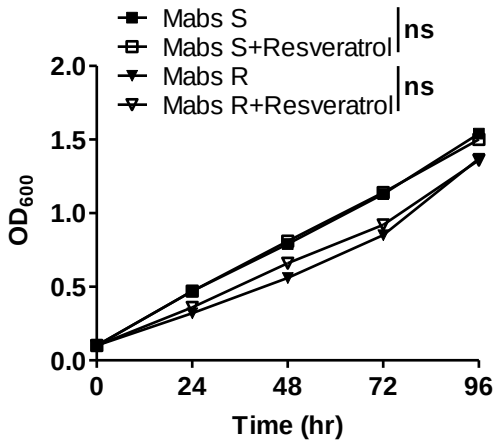

Supp Figure 4